Soft Matter

Rotational diffusion of colloidal microspheres near flat walls

Journal:	*Soft Matter*
Manuscript ID	SM-ART-10-2023-001320.R1
Article Type:	Paper
Date Submitted by the Author:	10-Jan-2024
Complete List of Authors:	Carrasco-Fadanelli, Virginia; Heinrich-Heine-Universitat Dusseldorf, Physics Mao, Yushan; Heinrich-Heine-Universitat Dusseldorf, Physics Nakakomi, Tomoki; Kyoto University Graduate School of Science Faculty of Science, Physics Xu, Haonan; Heinrich-Heine-Universitat Dusseldorf, Physics Yamamoto, Jun; Kyoto University Graduate School of Science Faculty of Science, Physics Yanagishima, Taiki; Kyoto University Graduate School of Science Faculty of Science, Physics Buttinoni, Ivo; Heinrich-Heine-Universitat Dusseldorf, Physics

Soft Matter

ARTICLE TYPE

Cite this: DOI: 00.0000/xxxxxxxxxx

Rotational diffusion of colloidal microspheres near flat walls

Virginia Carrasco-Fadanelli,[a] Yushan Mao,[a] Tomoki Nakakomi,[b] Haonan Xu,[a] Jun Yamamoto,[b] Taiki Yanagishima,*[b] and Ivo Buttinoni[a]

Received Date
Accepted Date

DOI: 00.0000/xxxxxxxxxx

Recently, colloids with an off-center fluorescent core and homogeneous composition have been developed to measure the rotational diffusivity of microparticles using 3D confocal microscopy in refractive index-matched suspensions. Here, we show that the same particles may be imaged using a standard fluorescence microscope to yield their rotational diffusion coefficients. Trajectories of the off-center core may be combined with known expressions for the correlation decay of particle orientations to determine an effective rotational diffusivity. For sedimented particles, we also find the rotational diffusivity about axes perpendicular and parallel to the interface by adding some bright field illumination and simultaneously tracking both the core and the particle. Trajectories for particles of different size yield excellent agreement with hydrodynamic models of rotational diffusion near flat walls, taking sedimentation-diffusion equilibrium into account. Finally, we explore the rotational diffusivity of particles in crowded two-dimensional monolayers, finding a different reduction of the rotational motion about the two axes depending on the colloidal microstructure.

1 Introduction

Since its first description on the basis of kinetic theory, it is widely known that the Brownian motion of spherical colloidal particles consists of both translational and rotational components. Similarly to hindered translational diffusion, rotational fluctuations are sensitive to interactions that might induce a torque on the particle, whether they be hydrodynamic, frictional or due to anisotropic force distributions. Even though measuring the rotational motion of microspheres is significantly more challenging than inferring their translation, a limited number of colloidal systems and techniques exist which allow for the characterization of rotational diffusivities. These methods include depolarized light scattering [1–3], fluorescence recovery [4], evanescent wave scattering [5,6], polarization microscopy [7,8], and digital tracking of particles with an anisotropic fluorescence profile or optical reflectivity [9–13].

Recently, chemically homogeneous core-shell microspheres with an off-center fluorescent core (OCULI) have been developed to track the orientation vector of spherical particles over time [14,15]. They are composed of 3-trimethoxysilyl propyl methacrylate (TPM), an organosilane widely applied in colloidal science to prepare a range of particle geometries with different functions [16–19]. These particles may be chemically modified post-synthesis to alter their surface properties, making them suitable as probes for a wide-range of surface interactions. Given the degree of interest in characterizing the frictional aspects of thermal colloidal particles in recent years [20], a facile means to measure the rotational diffusion of such probes would be a valuable addition to soft matter experiments. This particularly applies to model two-dimensional systems made of heavy colloidal microspheres that self-assemble on supporting substrates such as microscope glass slides [21]. While a number of experimental and theoretical studies elucidated how hydrodynamic interactions affect the translation Brownian motion of these colloidal building-blocks [22], the slowdown of the rotational motion of homogeneous spherical microspheres due to the underlying wall or neighbouring particles remains largely unexplored. However, the original OCULI suspension [14] was intended for two-channel three-dimensional laser scanning confocal microscopy, where the particles are suspended in index- and density-matched solvents.

In this work, we use OCULI to quantify the rotational diffusion of microspheres in water sedimented onto a flat surface, using a combination of conventional bright field and fluorescence microscopy. Analysis based on autocorrelation of the orientation vector yields not only an effective single-value rotational diffusivity, but also separate diffusivities about the axes parallel and perpendicular to the surface. In agreement with existing works, we find that the wall predominantly hinders the rotational motion around the axis parallel to it. We discuss the correspondence

[a] Institute of Experimental Physics of Condensed Matter, Heinrich-Heine University, Düsseldorf, Germany.
[b] Department of Physics, Graduate School of Science, Kyoto University, Kitashirakawa Oiwake-cho, Sakyo-ku, Kyoto 606-8502, Japan; E-mail: yanagishima.taiki.8y@kyoto-u.ac.jp

between our experimental measurements and theoretical predictions. We also investigate rotational diffusivities in assemblies of multiple particles in dense two-dimensional colloidal fluids and crystals. In the fluid phase, rotational motion is mainly weakened about the axis parallel to the wall, whereas all components are reduced in the crystalline structure. While the current work focuses on hydrodynamic interactions, the presented methods can be extended to probe any other particle-wall interaction that might impact the rotational diffusivity, such as surface roughness or transient stickiness.

2 Methods

2.1 Particle synthesis

The microspheres were prepared according to a procedure described previously[14]. Briefly, we prepare monodisperse TPM particles with a diameter of 1.0 μm (<5% polydispersity) fluorescently labeled with Cy3-NS succinimidyl ester preconjugated with 3-aminopropyltrimethoxysilane. These particles are dispersed in a dilute ammonia solution before slowly adding pre-hydrolyzed TPM solution. The additional TPM condenses onto the existing fluorescent particles, creating a non-fluorescent shell with a fluorescent core situated directly below the particle surface. Once the particles reach the desired size, 2,2'-azobis(isobutyronitrile) (AIBN) was added and the sample was heated to 80 degrees Celsius for 3 hours. Any secondary particles nucleated in the solution were separated by repeated centrifugation. These particles were named OCULI (Off-Center Under Laser Illumination) in previous works; we will also adopt this nomenclature and refer to the off-center core as the 'eye' of the colloid.

Since our goal is to achieve imaging of the dynamics of the core using standard optical microscopy, it is desirable to keep the fluctuations within a certain distance from the focal plane. Thus, when using larger particle sizes, we adopt a geometry where the OCULI particle is symmetrically coated by another non-fluorescent shell. This procedure is described in detail in previous work[14,23]. Briefly, Pluronic F108 is added to OCULI particles before crosslinking. This modifies the wetting properties of the surface such that additional pre-hydrolyzed TPM forms large lobes on the surface. The further addition of pre-hydrolyzed TPM before crosslinking leads to a smooth coverage of the original particle by a thick layer of non-fluorescent TPM on the surface. We refer to such particles as core-shell OCULI particles.

2.2 Sample preparation, imaging, and particle tracking

Before each experiment, OCULI particles are dispersed in Milli-Q water and sonicated for a few minutes to obtain a homogeneous suspension. The volume fraction, ε, depends on the particular experiment; the rotational diffusion of single particles is measured using very small particle concentrations ($\varepsilon \approx 0.008\%$), whereas larger volume fractions are used to investigate diffusivities in dense monolayer (here, the corresponding area fraction is extrapolated from the number of particles in the field of view). We pipette approximately 200 μl of colloidal suspension into a quartz sample cell (Hellma Analytics, Flow cell 137-QS, 1 mm height $\times$ 35 mm length $\times$ 9 mm width), seal the inlets and wait for the particles to entirely sediment onto the bottom substrate. Note, however, that physical contact between the TPM colloids and the quartz surface is inhibited by electrostatic repulsion since the two materials are negatively charged.

The sample cell is placed onto the stage of an inverted optical microscope (Olympus IX73) and illuminated by a halogen lamp and fluorescence light source (wavelength, $465-495$ nm), located respectively above and below the stage. While bright field illumination yields a diffraction-limited image of the particle itself, the fluorescence excitation selectively illuminates the position of the fluorescent 'eye' and makes it notably brighter than its surroundings. The focal depth of the 60X objective is such that the eye can be followed during the entire experiment, regardless of whether it is in the upper or lower hemisphere. We also verified that the Gaussian shape of the light emitted by the eye does not depend on its xy- or z-position, *i.e.* that the TPM matrix does not alter the fluorescence image. Videos are typically recorded at 5 frames per second using a CMOS camera (Orca Spark, Hamamatsu Photonics).

We then use in-house MATLAB algorithms to extract (ex-situ) the coordinates of the particle centers (PC) and eye centers (EC). To locate PC, we first binarize each frame using a low-pass filter so that only the dark edges of the particle are retained. We then flood-fill the background pixels and find the center of the circular regions using the Hough transform. EC are determined following the popular method of J. C. Crocker and D. G. Grier[24], *i.e.* by applying a band-pass filter that highlights the bright areas and locating the centers of the Gaussian intensity distributions. For single-particle experiments (Figs. 1-3), we only include in the analysis OCULI that are at least 5 radii apart. An example of EC and PC detection over time overlayed on microscopy images is given as a video (see Supplementary Information).

2.3 Determining the particle diffusivities

We follow the nomenclature of existing works[5] and define diffusion coefficients in the following way. (1) $D^t_{\parallel}$ is the translational diffusion coefficient of the particles in the xy-plane parallel to the wall. It is measured using the linear fit of the two-dimensional translational mean squared displacement (MSD) of PC ($MSD = 4D^t_{\parallel}\Delta t$, Δt being the delay time). (2) $D^r_{\parallel}$ and $D^r_{\perp}$ are the coefficients that characterize rotational diffusion about the axes parallel and perpendicular to the bottom surface, respectively. As we observe the particles using an objective placed just below the substrate, $D^r_{\perp}$ is determined from the azimuthal angle ϕ indicating the position of the 2D projection of EC onto the xy-plane with respect to the x-axis passing through PC (see sketch in Fig. 1a). Conversely, $D^r_{\parallel}$ is obtained from the projection onto the xz-plane (details below). Note that the polar angle θ required for this projection is extracted using the distance l between the 2D-projections of PC and EC (Fig. 1a), an approach that is possible because the focal depth of the imaging objective is larger than 2R and the fluorescence intensity profile is not affected by the TPM matrix.l takes values between 0 (if EC overlaps with PC) and the radius of rotation r_{rot} of EC with respect to PC, given by the difference between the radius of the particle and the

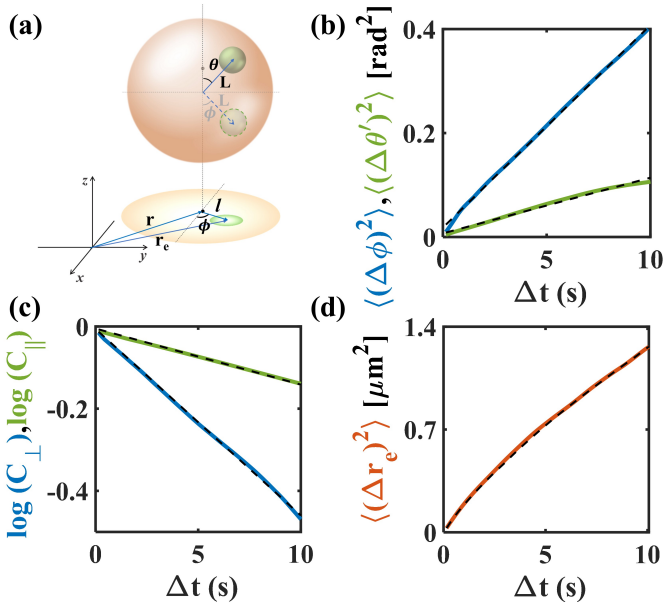

Fig. 1 (a) Schematic illustration of the angles and positions used to measure rotational and translational diffusivities. $D^r_\perp$ is extracted from θ and $\mathbf{r}$. $D^r_\parallel$ is extracted from l and $\mathbf{r}$. D^r_{eff} is extracted from $\mathbf{r}$ and $\mathbf{r_e}$. $D^t_\parallel$ is extracted from $\mathbf{r}$. (b) Mean squared angular displacements $\langle(\Delta\phi)^2\rangle$ and $\langle(\Delta\theta')^2\rangle$ corresponding to rotational diffusion about the axes normal (blue) and parallel (green) to the quartz substrate, respectively. The dashed lines are linear fits. (c) Log of the average auto-correlation function of the orientation vectors and linear fitting curves (dashed lines). (d) Two-dimensional mean squared displacement of EC and fitting curve given by Eq. (4). The curves in (b-d) are obtained for particles of radius $R = 2.3\ \mu$m.

one of the eye (minus, eventually, the thickness of the additional non-fluorescent shell). Note that the minimum tracking resolution required for this technique to work is largely determined by whether this distance is resolvable. Trajectories must be corrected for periodicity to yield continuous, unconfined time series. As the angles ϕ and θ are analyzed over time, their value may also evolve in an unphysical manner. This happens for instance when EC reaches the top of the particle and diffuses out at a completely different azimuthal angle, or when EC moves between the top and bottom hemisphere of the particle (in 2D microscopy the two hemispheres are indistinguishable). In practice, we record videos that are approximately twenty minutes long, and reset ϕ (θ) each time the xy-projection of EC is near the particle center (edge). For spheres, this is possible because the rotational behavior does not depend on the orientation. Finally, the measurement of $D^r_\parallel$ requires the buoyant weight of the particle to prevent significant oscillations in z (see also Section 4).

With these caveats fulfilled, we adopt two separate approaches in order to calculate the rotational diffusivity of particles sedimented onto the glass surface. One method is shown in Fig. 1b: it consists of finding the mean squared angular displacements for the orientation angle of the particle on two different planes. Given a conventional representation of the orientation vector in spherical coordinates $\mathbf{u} = (\sin\theta\cos\phi, \sin\theta\sin\phi, \cos\theta)$, as shown in Fig.1(a), the vector may be projected on to the xy and xz planes and re-normalized, yielding orientation angles with respect to the x and z axes respectively. Note that the orientation with respect to the x-axis is the same as the azimuthal angle ϕ, but the angle with respect to the z-axis θ' is not equal to the polar angle θ, but modified such that $\tan\theta' = \tan\theta\cos\phi$. This yields two measures of rotational diffusion about different axes, $\langle(\Delta\phi)^2\rangle$ (blue line) and $\langle(\Delta\theta')^2\rangle$ (green line). Fitting them (dashed lines) according to

$$\langle(\Delta\phi)^2\rangle = 2D^r_\perp \Delta t, \quad \langle(\Delta\theta')^2\rangle = 2D^r_\parallel \Delta t, \tag{1}$$

we can extract $D^r_\perp$ and $D^r_\parallel$.

Alternatively, the rotational diffusion coefficients are obtained from the auto-correlation functions $C_\perp(\Delta t)$ and $C_\parallel(\Delta t)$. In the absence of external torques, $C_\perp$ and $C_\parallel$ decay exponentially as

$$\begin{aligned} \langle C_\perp(\Delta t)\rangle &= \langle\cos(\phi(t_2) - \phi(t_1))\rangle = e^{-2D^r_\perp \Delta t} \\ \langle C_\parallel(\Delta t)\rangle &= \langle\cos(\theta'(t_2) - \theta'(t_1))\rangle = e^{-2D^r_\parallel \Delta t} \end{aligned} \tag{2}$$

for $\Delta t = t_2 - t_1$ (Fig. 1c, where we use the same color code as in Fig. 1b). Rotational diffusivities calculated using either of the two methods are statistically identical. We note that a similar projection was adopted by Kamp *et al.*[15] using two-color confocal microscopy images of particles with the same fluorescence profile, confined in a 2D colloidal crystal.

However, in many applications, the precise measurement of the relative position of EC to PC is challenging and time-consuming. For example, even bright field illumination via transmission may not be possible due to containment constraints. Thus, we also introduce an alternative means of extracting an effective rotational diffusion coefficient (D^r_{eff}) exclusively from the xy-position of EC, without any information about the instantaneous orientation vector. Here, we assume that the rotational and translational diffusion of the particle are decoupled and consider diffusion in the position of the eye given by $\mathbf{r_e} = \mathbf{r_p} + r_{\text{rot}}\mathbf{u}$, where $\mathbf{r_p}$ is the position of PC, $\mathbf{u}$ is the orientation unit vector defined by the position of the eye relative to the center. As above, the auto-correlation of $\mathbf{u}$ is known to decay exponentially in the absence of torques as

$$\langle C_{\text{eff}}(\Delta t)\rangle = e^{-2D^r_{\text{eff}}\Delta t} \tag{3}$$

where D^r_{eff} is the rotational diffusivity of the particle, assuming isotropic rotational motion about all axes. Combining this and our knowledge of the two-dimensional mean-squared displacement of PC, *i.e.* conventional translational diffusion, we obtain the following expression for the (translational) mean squared displacement of EC (Fig. 1d):

$$\langle \Delta\mathbf{r_e}^2\rangle = 4D^t_\parallel \Delta t + \frac{4}{3}r^2_{\text{rot}}(1 - e^{-2D^r_{\text{eff}}\Delta t}) \tag{4}$$

Note that in the long-time limit, the rotational contribution disappears and $\langle \Delta\mathbf{r_e}^2\rangle$ becomes a line intercepting the y-axis at $\frac{4}{3}r^2_{\text{rot}}$. A more detailed derivation is given in the Supplementary Material.

2.4 Theoretical predictions for hydrodynamic interactions

A vital part of validating our method is a quantitative comparison with hydrodynamic models for translational and rotational

mobility of particles in the vicinity of a hard wall. For this, we adopt the Pade approximant proposed by Cicochki and Jones[25] for friction functions using coefficients up to the tenth order[26]. This numerical representation allows accurate determination of mobility functions of particles in the vicinity of a wall, including up to the asymptote at particle-wall contact. Note that the functions calculated by Jones *et* al. are functions of the inverse of the particle-wall distance, scaled by the particle size. For calculations requiring a smooth function of different diffusivities at arbitrary particle-wall distances, we adopt a cublic spline for interpolation.

3 Experimental Results

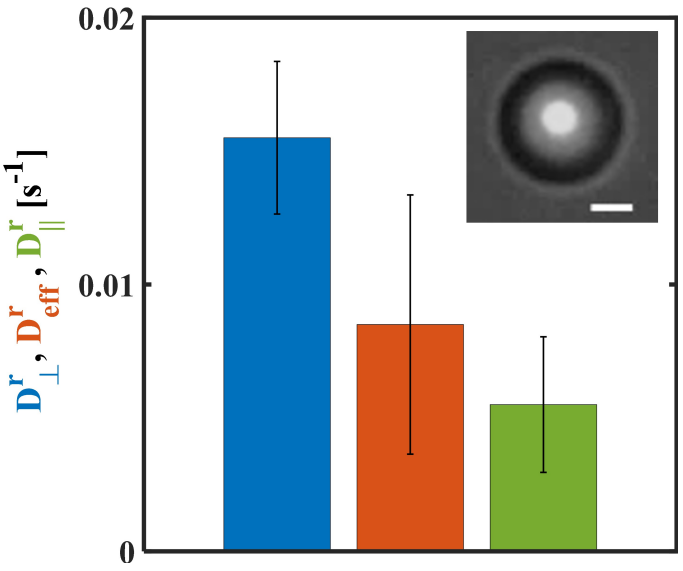

Fig. 2 Rotational diffusion coefficients, as defined in the main text, of OCULI microspheres ($R = 2.3$ μm) located near a flat quartz wall and imaged in 2D using a combination of fluorescence and bright-field microscopy (inset). The scale bar corresponds to 2 μm. The values of $D^r_\parallel$, $D^r_\perp$ and D^r_{eff} are an average over approximately 100 particles and the error bars correspond to the standard deviation of the data.

We first report the diffusivity of single OCULI spheres of radius $R = 2.3 \pm 0.04$ μm suspended in water after they sedimented onto a quartz substrate (see inset in Fig. 2). The translational diffusion coefficient is found to be $D^t_\parallel = 0.054 \pm 0.011$ μm^2/s. Rotational diffusion coefficients $D^r_\perp$ (blue data), $D^r_\parallel$ (green data) and D^r_{eff} (orange data), as defined in Section 2, are given in Fig. 2. All diffusion coefficients are smaller or similar to the bulk values given by the Stokes-Einstein relations, $D^t_{SE} = k_B T/(6\pi\eta R) = 0.095$ μm^{2}s^{-1} and $D^r_{SE} = k_B T/(8\pi\eta R^3) = 0.013$ s^{-1}. In particular, because the hydrodynamics is hindered by the presence of the wall, $D^r_\parallel$ is significantly smaller than $D^r_\perp$, indicating that the particle rotates faster about the z-axis than it does around axes parallel to the wall. We also note that D^r_{eff} constitutes an intermediate value that characterizes both diffusivities. In effect, this is a single term approximation to an orientational relaxation characterized by two time scales. In the absence of information on particle centers, this would constitute a representative single-value characterization of rotational diffusivity.

To address how the hindered diffusivity of microparticles near

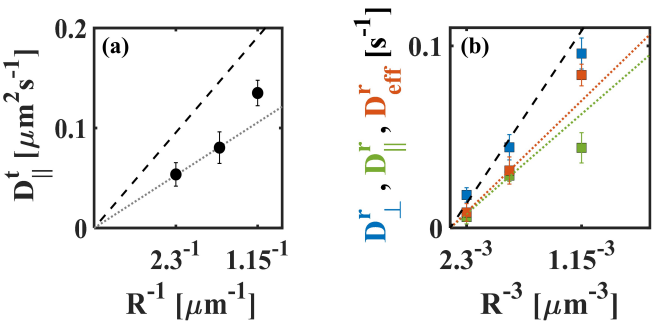

Fig. 3 (a) Translational and (b) rotational diffusion coefficients for OCULI particles of different size, plotted as a function of R^{-1} and R^{-3}, respectively. $D^t_\parallel$, $D^r_\parallel$, $D^r_\perp$ and D^r_{eff} are defined in the main text. The dashed lines correspond to the SE predictions for bulk diffusivities. The dotted lines correspond to linear fits crossing the origin for particles with $R = 1.5$ μm and $R = 2.3$ μm (first two data points). Each measurement is an average over 100 particles and the error bars correspond to the standard deviation of the data.

planar confinements depends on their dimension, we then measured $D^t_\parallel$, $D^r_\parallel$ and $D^r_\perp$ for two additional batches of OCULI of radius $R = 1.15$ μm and $R = 1.5$ μm. In bulk, D^t_{SE} and D^r_{SE} scale linearly with R^{-1} and R^{-3}, respectively, and the slope of these lines gives the viscosity η of the surrounding fluid at a given temperature (here, room temperature). This linear behaviour is highlighted by the black dashed lines in Fig. 3a and Fig. 3b, together with our experimental data of OCULI undergoing Brownian motion just above the quartz surface. For all sizes, the underlying substrate significantly reduces $D^t_\parallel$, $D^r_\parallel$ and D^r_{eff}. $D^r_\perp$ is only weakly affected by the confinement, in agreement with theoretical predictions[6]. Interestingly, the data that correspond to the two largest particles ($R = 2.3$ μm and $R = 1.5$ μm) can be also accurately fitted by linear functions that cross the origin (see for instance the dotted lines in Fig. 3a and Fig. 3b), but have a slope smaller than the Stokes-Einstein predictions (dashed lines). This suggests that the particles are approximately located at the same height with respect to the substrate – likely determined by electrostatic repulsion – and experience the same 'local viscosity' as a result of both the aqueous medium and neighbouring wall. However, this 'viscosity' is conditional to the type of motion under investigation: rotational diffusion in xy ($D^r_\perp$) sees an environment that is less viscous than the one experienced upon translational Brownian motion ($D^t_\parallel$). The smallest OCULI defy this behaviour. $D^t_\parallel$ (Fig. 3a) and D^r_{eff} (Fig. 3b, orange data) lie significantly above the dotted line, whereas $D^r_\parallel$ (Fig. 3b, green data) is much smaller than what is expected from the Stokes-Einstein behaviour. These seemingly contradicting results highlight the limitation of the method used to determine $D^r_\parallel$ and will be discussed in detail in Section 4.

As a further test for our methods, we examined the rotational diffusion of the OCULI particles shown in Fig. 2 ($R = 2.3$ μm), when they self-assemble into a dense liquid (area fraction $\phi \approx 0.42$, see panel (ii) in Fig. 4) and crystalline monolayers (area fraction $\phi \approx 0.61$, see panel (iii) in Fig. 4). Note that, at $\phi \approx 0.61$, the two-dimensional microstructure is polycrystalline,

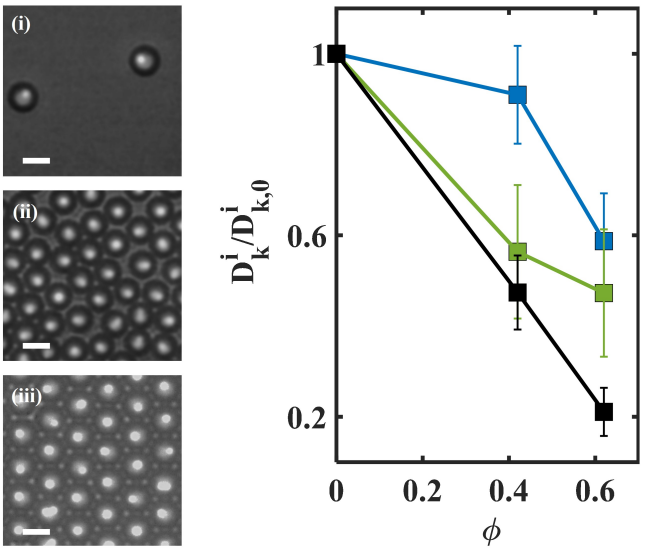

Fig. 4 $D^t_{\parallel}$ (black), $D^r_{\perp}$ (blue), $D^r_{\parallel}$ (green) of OCULI particles ($R = 2.3\ \mu$m) diffusing near a flat solid substrate, plotted as a function of the local area fraction ϕ. All diffusion coefficients are normalized by the corresponding diffusivities in the dilute limit ($\phi \approx 0$). For simplicity, in the y-label we use the following nomenclature: $k = \{\parallel, \perp\}$ and $i = \{t, r\}$. The panels on the left-hand side are the microscopy images at (i) $\phi \approx 0$, (ii) $\phi \approx 0.42$ and (iii) $\phi \approx 0.61$. Each data point is an average over 100 particles. The scale bars are 5 μm.

but we only look at particles located inside crystalline domains (particles surrounded by six neighbours). The plot in Fig. 4 depicts how rotational ($D^r_{\perp}$ and $D^r_{\parallel}$) and translational ($D^t_{\parallel}$) diffusion slow down due to an increase of particle concentration. To tackle the role of hydrodynamic interactions, we only consider the short-time translational diffusivities, *i.e.* time intervals for which the mean squared displacement displays diffusive behaviour. $D^t_{\parallel}$ shows an approximate linear decrease as function of the area fraction, in qualitative agreement with previous works of colloidal monolayers on solid substrates[22]. The weakening of rotational Brownian motion is more complex and, to our knowledge, unexplored. As the monolayer reaches the dense liquid phase ($\phi \approx 0.42$), the presence of neighbouring particles predominantly affects the rotational diffusion about the axis parallel to the substrate $D^r_{\parallel}$ (green data), whereas $D^r_{\perp}$ (blue data) only displays a slight decrease. The opposite happens when we further quench the system into crystalline microstructures with hexagonal order ($\phi \approx 0.61$): now rotational diffusion is mainly reduced about the axis perpendicular to the wall ($D^r_{\perp}$, blue data). At $\phi \approx 0.61$, $D^r_{\perp}$ and $D^r_{\parallel}$ have undergone the same slowdown compared to their diluted value. Overall, a clear disparity can be seen in their dependence on ϕ (Fig. 4).

4 Discussion

Due to symmetry considerations, tracking the rotational diffusion of spherical micro- and nanoparticles is a challenging task. The last two decades have witnessed the development of a range of techniques to infer rotational fluctuations as efficiently as it has been done for translational Brownian diffusion. Most of these methods, if not all, require complicated experimental setups and/or data analysis. Scattering experiments call, for instance, for a thorough understanding of the light-scattering signals and can be only applied to particles that are sufficiently small (< 1 μm). Instead, the rotational motion of microparticles is usually observed by introducing surface patches and tracking their displacement over time in optical-microscopy setups. The limitations are that surface patches often modify the properties of the particle (e.g. its weight distribution[11]) and confocal experiments are usually needed to extract the three-dimensional rotational motion. Very recently, Niggel and coworkers proposed a new method based on standard epifluorescence microscopy and image correlation to follow the full short-time rotational displacement of raspberry microspheres[13]. It is also worth mentioning previous works which used spherical particles enveloping an asymmetric centered fluorescent core such as an ellipse[10] or a fluorescent cluster[12], as their scope of application is very similar to ours. These elegant techniques, particularly the former, reduce the complexity of the experimental setup, very much in the spirit of this work, but still carries higher computational costs during ex-situ analysis.

Here, we presented a facile and intuitive method to measure the rotational diffusivity of spherical microparticles that are equipped with an off-center fluorescent core and quasi-confined in two dimensions. Epifluorescence microscopy alone can be employed to determined an effective rotational diffusivity, under the assumption that translational and orientational diffusion are decoupled. The addition of bright-field illumination gives full access to the rotational diffusion coefficients about the axis parallel and perpendicular to the plane of translational motion. Our approach has several *advantages*. (1) The particles have homogeneous composition and surface properties since the 'eye' is made of the same material of the particle and embedded inside. (2) The effective rotational diffusivity can be extracted as easily as any translational diffusion coefficient and measured even if the particles are not confined in 2D. (3) The computational cost for the measurement of $D^r_{\perp}$ and $D^r_{\parallel}$ is very low (only two positions must be tracked for each particle: EC and PC) and uses widely available particle tracking algorithms. Deployment is trivial to arbitrarily dense suspensions. (4) The experimental setup consists of a simple epifluorescence microscope. We applied our experimental protocols to the problem of spherical colloids diffusing just above flat solid substrate, which – surprisingly – has been only marginally addressed for particles in the micron size range. The measurements indicate that the underlying wall slows down the rotational diffusion in an asymmetric fashion, with the rotation about the axes parallel to the surface being the most affected. This result is in full agreement with experiments investigating nanoparticles.

We may go further in our analysis and consider the quantitative consistency of the diffusivities found experimentally with theoretical predictions, taking into account the hydrodynamic torque exerted by the wall onto the particle. Details of the calculation are given in the Methods section. Firstly, the model yields estimates for rotational and translational diffusivities for a particle in asymptotic proximity to a wall. In the absence of additional interactions between the particle and wall such as adhesion or

roughness-induced friction, this would constitute a lower bound for any diffusivity found (solid lines in Fig. 5). Importantly, this value is found independently of any fit parameters. Superimposing both the ultra-dilute upper limit found via the SE equation (dashed lines in Fig. 5 – only shown in the left panel for clarity) and the contact lower limit on the translational and rotational diffusivities found for different particle sizes, we find that our experimental values lie within these bounds (Fig. 5). Note that, for the most part, the experimentally found diffusivities are larger than the ones predicted for particle contact. This is likely due to two effects. The first is sedimentation-diffusion (SD) equilibrium; thermal fluctuations may displace the particle in the z-direction, allowing the particle to explore positions where the diffusivity may be slightly higher. We may approximate the effect of sedimentation-diffusion by calculating an effective diffusivity:

$$\langle D^{t,r}\rangle_{SD} = \frac{\int_a^\infty dz D^{t,r}(z)\exp(-z/l_g)}{\int_a^\infty dz \exp(-z/l_g)}, \quad (5)$$

where l_g is the gravitational length of the particles, following the approach adopted in[6]. Integration limits for this function are taken to be at least 200 times the particle radius. Equation (5) is shown by the dotted lines in Fig. 5. This averaged diffusivity bridges the two limits discussed above, as the particle is expected to be unconfined when it is very light, and confined to surface contact when it is very heavy. The trend of smaller particles exhibiting a larger than expected diffusivity is reflected both in the transitional form of the predicted curve, and the experimentally measured diffusivities, particularly $D^t_\parallel$. The quantitative discrepancy in $D^t_\parallel$ is most likely due to electrostatic repulsion between the particle and the surface. Given that double distilled water exposed to the atmosphere of the lab can have a Debye length on the order of hundreds of nanometers, it is reasonable to assume that the particles maintain some distance from the base, leading to an increased mobility. Interestingly, we also find excellent agreement between both components of rotational diffusivity and theoretical estimates (Fig. 5b), seemingly highlighting a decoupling between translational and rotational mobilities. In the absence of a detailed model for particle-surface interactions, we note that a crude approximation to a long-ranged repulsion may be made by introducing a hard-wall repulsion at some nominal 'particle-wall' separation distance and incorporating this into the integration limits of equation (5). For the three particle sizes we used, we use the experimentally determined D^t to approximate the wall position, i.e. an estimation of the distance from the particle to the glass surface. From the smallest to largest size, we obtain a separation of 0.82, 0.31 and 0.66 microns. These are all approximately consistent with the Debye length of ultrapure water.

The anomalous measurement which defies both theoretical predictions and trends is the smallest particle size measurement of $D^r_\parallel$, which is significantly reduced (Fig. 5b, green data point on the far right). This highlights an important limitation of our method, which is an ambiguity introduced into the trajectory of the eye when generating projected orientation vectors to find $D^r_\parallel$. When the particle is so light that there is significant posi-

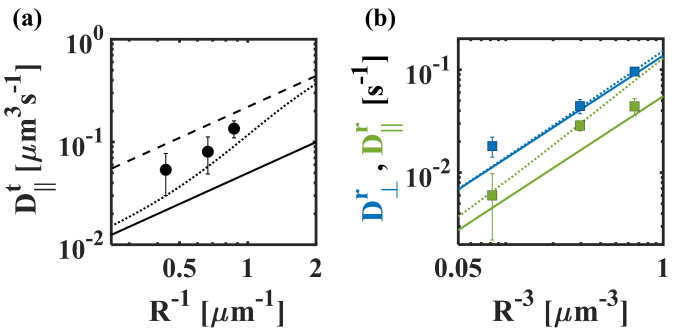

Fig. 5 (a) Translational and (b) rotational diffusion coefficients for OCULI particles of different size, plotted as a function of R^{-1} and R^{-3}. Diffusion coefficients are color coded $D^t_\parallel$ (black), $D^r_\parallel$ (green) and $D^r_\perp$ (blue), the same as in Fig. 3. Dotted lines are theoretical predictions based on the hydrodynamic torque exerted by the wall onto the particles with sedimentation-diffusion equilibrium. Solid lines indicate theoretical predictions for a lower limit, assuming asymptotic contact between the particle and the wall. The dashed line in (a) correspond to the Stokes-Einstein prediction for a particle in the ultra-dilute limit.

tional fluctuation in z (on the order of the particle size), the z-component of the orientation vector diverges from what might be expected when we assume that the particle is stationary in the z-direction (like when a heavy particle is sedimented on the surface). Thus, successful extraction of axis-dependent rotational diffusivity is largely limited to particles which are heavy enough such that they do not fluctuate strongly in z. While z fluctuations can affect measurements of $D^r_\parallel$, we stress that the accuracy of D^r_{eff} is not compromised, so long as the rotational motion is diffusive. We may demonstrate this by measuring the mean-squared displacements of ECs of OCULI particles dispersed in an approximately density-matching solvent, where z fluctuations are expected to be just as large as those in x and y. Fitting with equation (4) gives translational and rotational diffusivities consistent with those expected in bulk at infinite dilution (see Supplementary Material). This makes measurement feasible any anywhere the particle eye may be individually resolved.

Finally, we briefly consider our measurement of axis-dependent rotational diffusivities in dense monolayers. Measurements of single value rotational diffusivity in dense monolayers of spherical particles has been achieved using Janus particles with anisotropic interactions as well as optical anisotropy[27], but to our knowledge, axis dependent measurements of purely hydrodynamic effects in such dense monolayers, both liquid-like and crystalline, are yet to be explored. We stress that this was enabled by the unique geometry of OCULI particles, a single, unambiguously located off-center core for each particle which may be projected to different planes to yield axis-dependent orientations. As noted previously, it is clear from Fig.4 that the degree to which D^r changes with area fraction depends on both the rotation axis and phase. While each colloid can be viewed as an additional 'wall' for its neighbours, if the monolayer is liquid-like, OCULI are still free to move in the xy-plane and thus present a 'mobile' wall. This is not the case when the microstructure is solid-like (crystalline), though neighbours may still show some thermal fluctuations. Further

experiments varying the particle concentration are needed to understand the role of fixed and mobile obstacles in hindering the rotational diffusion of microscopic particles; but while these measurements are beyond the scope of the current manuscript, we note that the diffusivity disparity between axes is something that should be considered when coarse-grained approaches are taken to incorporate hydrodynamics into simulations of colloidal monolayers, like crowded proteins near a membrane or wall.

5 Conclusions

We introduced a method for measuring the rotational diffusivity of particles with a single, fluorescent, off-center core sedimented onto a flat surface. The method is highly intuitive and may be easily realized by any investigator with access to a fluorescence microscope and standard, freely available particle tracking algorithms. We demonstrated both an estimate based solely on the trajectory of the fluorescent eye, and a fuller characterization taking different diffusivities about axes parallel and perpendicular to the surface into account. Both are shown to give reliable, consistent measurements. The experimentally found diffusivities for different sized particles are found to broadly agree with theoretical estimates based on a hydrodynamic interaction with the surface and sedimentation-diffusion. Finally, a measurement of particles in a dense monolayer on the surface reveal a selectively suppressed $D^r_{\parallel}$, showing that even the 'mobile walls' introduced by neighboring particles can have a measurable effect. The many-body hydrodynamic effect that this arises from would constitute interesting further work, particularly in the context of inter-particle dynamical coupling in dense confinement.

Coupled with ease of particle synthesis and functionalization, we believe the system has the potential to allow for the characterization of diffusion in a wide range of contexts, from the investigation of surface interactions in biochemical experiments e.g. on lipid bilayers, liquid-liquid interfaces etc., to the characterization of effective diffusivities when translational motion is strongly suppressed, e.g. in the actively circulating environment of biological cells. We note that the framework which we introduce may also be applied to non-spherical particles, so long as some identification of orientation is available[28,29].

Author Contributions

Contributions were as follows according to the CRediT framework. Authors are given by order of appearance in the author list. Conceptualization (TY, IB); Data Curation (VC-F, YM, TN, HX); Formal Analysis (VC-F, YM, HX, TY, IB); Funding Acquisition (TY, IB, JY); Investigation (all authors); Methodology (VC-F, TN, TY); Software (VC-F, TY); Supervision (TY, IB, JY); Validation (VC-F, YM, TN, TY, IB); Visualization (VC-F, TY, IB); Writing - Original Draft (VC-F, TY, IB); Writing - Review and Editing (all authors).

Conflicts of interest

There are no conflicts of interests to declare.

Acknowledgements

We thank Roel Dullens for inspiring discussions. IB acknowledges Heinrich-Heine University and the German Research Foundation for funding. TY acknowledges a Toyota Riken Scholar Grant, Kyoto University, and the Kyoto University Foundation for financial support. TY and JY also acknowledge JST-CREST Grant Number JPMJCR2095.

Notes and references

1 V. Degiorgio, R. Piazza, U. Pavia and R. B. Jones, *Phys. Rev. E*, 1995, **52**, 2707–2717.
2 G. H. Koenderink and A. P. Philipse, *Langmuir*, 2000, **16**, 5631–5638.
3 A. Mertelj, J. L. Arauz-Lara, G. Maret, T. Gisler and H. Stark, *Europhys. Lett.*, 2002, **59**, 337–343.
4 M. P. Lettinga, G. H. Koenderink, B. W. M. N. Kuipers, E. Bessels and A. P. Philipse, *J. Chem. Phys.*, 2004, **120**, 4517–4529.
5 S. A. Rogers, M. Lisicki, B. Cichocki, J. K. G. Dhont and P. R. Lang, *Phys. Rev. Lett.*, 2012, **109**, 098305.
6 M. Lisicki, B. Cichocki, S. A. Rogers, J. K. G. Dhont and P. R. Lang, *Soft Matter*, 2014, **10**, 4312–4323.
7 S. Martin, M. Reichert, H. Stark and T. Gisler, *Phys. Rev. Lett.*, 2006, **97**, 248301.
8 F. Giavazzi, C. Haro-Pérez and R. Cerbino, *J. Phys.: Condens. Matter*, 2016, **28**, 195201.
9 S. M. Anthony, L. Hong, M. Kim and S. Granick, *Langmuir*, 2006, **22**, 9812–5.
10 M. K. Klein, N. Klinkenberg, S. Schuetter, N. Saenger, P. Pfleiderer and A. Zumbusch, *Langmuir*, 2015, **31**, 2655–2661.
11 B. Liu and A. Böker, *Soft Matter*, 2016, **12**, 6033–6037.
12 S. Schütter, J. Roller, A. Kick, J.-M. Meijer and A. Zumbusch, *Soft Matter*, 2017, 8240–8249.
13 V. Niggel, M. R. Bailey, C. van Baalen, N. Zosso and L. Isa, *Soft Matter*, 2023, **19**, 3069–3079.
14 T. Yanagishima, Y. Liu, H. Tanaka and R. P. A. Dullens, *Phys. Rev. X*, 2021, **11**, 021056.
15 M. Kamp, B. de Nijs, J. J. Baumberg and O. A. Scherman, *J. Colloid Interface Sci.*, 2021, **581**, 417–426.
16 S. Sacanna, W. T. Irvine, P. M. Chaikin and D. J. Pine, *Nature*, 2010, **464**, 575–578.
17 Y. Wang, X. Zheng, E. Ducrot, J. S. Yodh, M. Weck and D. J. Pine, *Nat. Commun.*, 2015, **6**, 7253.
18 T. Hueckel and S. Sacanna, *ACS Nano*, 2018, **12**, 3533–3540.
19 Z. Xu, T. Hueckel, W. T. Irvine and S. Sacanna, *Nature*, 2021, **597**, 220–224.
20 L. C. Hsiao and S. Pradeep, *Curr. Opin. Colloid Interface Sci.*, 2019, **43**, 94–112.
21 A. L. Thorneywork, J. L. Abbott, D. G. A. L. Aarts and R. P. A. Dullens, *Phys. Rev. Lett.*, 2017, **118**, 158001.
22 A. L. Thorneywork, R. E. Rozas, R. P. A. Dullens and J. Horbach, *Phys. Rev. Lett.*, 2015, **115**, 268301.
23 Y. Liu, K. V. Edmond, A. Curran, C. Bryant, B. Peng, D. G. A. L.

Aarts, S. Sacanna and R. P. A. Dullens, *Adv. Mater.*, 2016, **28**, 8001–8006.

24 J. C. Crocker and D. G. Grier, *J. Colloid. Interface Sci.*, 1996, **179**, 298–310.

25 B. Cichocki and R. B. Jones, *Phys. A: Stat. Mech. Appl.*, 1998, **258**, 273–302.

26 G. S. Perkins and R. B. Jones, *Phys. A: Stat. Mech. Appl.*, 1991, **171**, 575–604.

27 S. Jiang, J. Yan, J. K. Whitmer, S. M. Anthony, E. Luijten and S. Granick, *Phys. Rev. Lett.*, 2014, **112**, 1–5.

28 T. H. Besseling, M. Hermes, A. Kuijk, B. De Nijs, T. S. Deng, M. Dijkstra, A. Imhof and A. Van Blaaderen, *J. Phys.: Condens. Matt.*, 2015, **27**, year.

29 J. Roller, P. Pfleiderer, J.-M. Meijer and A. Zumbusch, *J. Phys.: Condens. Matter*, 2018, **30**, 395903.